

# Boosting Thermodynamic Efficiency with Quantum Coherence of Phaseonium Atoms

Federico Amato,<sup>1,2,\*</sup> Gerardo Adesso,<sup>2,†</sup> G. Massimo Palma,<sup>3</sup> Salvatore Lorenzo,<sup>3</sup> and Rosario Lo Franco<sup>1,‡</sup>

<sup>1</sup>*Dipartimento di Ingegneria, Università degli Studi di Palermo, Viale delle Scienze, 90128 Palermo, Italy*

<sup>2</sup>*School of Mathematical Sciences and Centre for the Mathematics and Theoretical Physics of Quantum Non-Equilibrium Systems, University of Nottingham, University Park, Nottingham NG7 2RD, UK*

<sup>3</sup>*Dipartimento di Fisica e Chimica - Emilio Segrè, Università degli Studi di Palermo, Via Archirafi 36, I-90123 Palermo, Italy*

(Dated: March 12, 2026)

We present a realistic implementation of a quantum engine powered by a phaseonium gas of coherently prepared three-level atoms—where quantum coherence acts as a thermodynamic resource. Using a collision model framework for phaseonium-cavity interactions and cavity optomechanics, we construct a full engine cycle based on two non-thermal reservoirs, each characterized by coherence-induced effective temperatures. This configuration enhances the efficiency of a simple optomechanical engine operating beyond standard thermal paradigms. We further address scalability by coupling a second cavity in cascade configuration, where the same phaseonium gas drives both cycles. Our results demonstrate the operational viability of coherence-driven quantum engines and their potential for future thermodynamic applications.

Quantum thermodynamics extends classical thermodynamic principles to the microscopic quantum realm, exploring how quantum effects like coherence and entanglement influence the operation of thermal machines. Quantum coherence is indeed considered as a new *resource* for thermodynamics tasks [1–3]. Coherent states are non-thermal states, where coherences are represented in the density matrices of the system by nonzero values of off-diagonal elements. When used as environment, coherent systems may be characterized by “local” or “apparent” temperatures [4, 5], to which the working fluid thermalizes at the equilibrium. In particular, only coherences between degenerate levels can influence the apparent temperature of quantum systems [5–8]. To this aim, *phaseonium* [9] is the minimum viable system to show this property. Phaseonium is a gas of three-level atoms in V or  $\Lambda$  configuration with coherence between the degenerate excited or ground states. It is considered as an unconventional “state of matter” that displays genuine quantum features, from the optical [9–12] to the thermodynamic [13, 14] domain. Different proposals of quantum engines use phaseonium as quantum reservoir [13, 15, 16]: in fact, gauging its coherence phase, one can control the temperature to which a cavity field in contact with it thermalizes. Optomechanical cavities [17] are being widely explored as quantum engines, where radiation pressure can be used to move one mirror like a piston back and forth heating and cooling the cavity. Previous models present idealized, approximated results for the efficiency of the engines, focusing on impractical Carnot cycles, where the level spacing of atoms should be continuously changed to keep them resonant with a moving cavity.

In this Letter, we propose the implementation of a realistic quantum engine in a cavity optomechanical platform, fuelled by phaseonium atoms. We compute its performance using a collision model framework [18], which provides the *exact* dynamics of a cavity in contact with phaseonium atom [14], along with an analytical expression of the equilibrium temperature reached by the cavity. In the spirit of Ref. [19], we track heat and work exchanged during one cycle and compute the *efficiency* of the engine, highlighting the role of quantum co-

herence in enhancing work extraction. We then address the problem of *scalability* by adding a second cavity in a cascade configuration, where phaseonium atoms drive the cycle in both cavities. Figure 1 shows an ideal setup.

Our results provide the first thermodynamically consistent description of a phaseonium-powered optomechanical engine, revealing a direct operational link between microscopic quantum systems and macroscopic mechanical work. More generally, our approach establishes a framework for scalable quantum thermal machines with tunable environments, offering a simple platform well-suited for experimental realizations in cavity QED and optomechanical systems.

*Model*— Our system consists of two optical cavities in cascade configuration, interacting with a beam of three-level phaseonium atoms, as shown in Fig. 1(c).

The two cavity fields,  $S_1$  and  $S_2$ , are modelled as standard single mode harmonic oscillators [20], with a controllable interaction with a stream of phaseonium as quantum reservoirs. The coherent state that defines phaseonium atoms can be represented by the density operator presented in Fig. 1(a), with the normalization condition  $|\alpha|^2 = 1 - |\beta|^2$ . We choose a resonant coupling for the cavities and atoms frequencies and use the interaction picture to leave the free evolution of both the cavity and the bath out of the analysis. We use the collision model to study the thermalization dynamics of the systems interacting with the phaseonium. This is a thermalization process to an apparent temperature given by phaseonium atoms’ coherences and populations:

$$k_B T_\phi = \frac{\hbar\omega}{\ln\left(\frac{\beta^2(1-\sin\phi)}{2\alpha^2}\right)}, \quad (1)$$

For comparison, the master equation for a cavity interacting with a thermal (diagonal) three-level atom in  $\Lambda$  configuration—without quantum coherence—leads to a stable temperature for the cavity

$$k_B T_{cl} = \frac{\hbar\omega}{\ln\left(\frac{\beta^2}{2\alpha^2}\right)}. \quad (2)$$

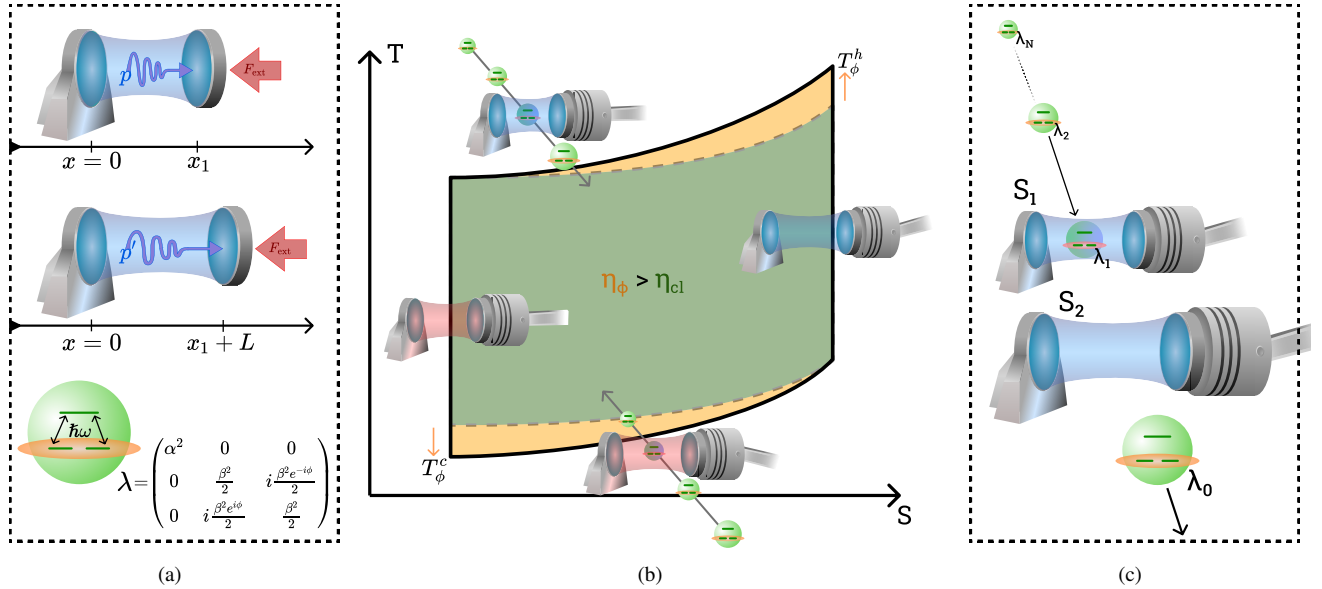


FIG. 1. Quantum heat engine architecture. (a) The working medium consists of a single-mode optical cavity with a movable end mirror, allowing the cavity length to vary from  $x_1$  to  $x_1 + L$  under the influence of radiation pressure. The cavity interacts with a stream of three-level atoms in  $\Lambda$  configuration, characterized by partial coherence in the ground-state subspace and represented by the density matrix  $\lambda$ . These atoms serve as a tunable quantum reservoir. (b) Thermodynamic Otto cycle plotted in the entropy–temperature ( $S$ – $T$ ) plane. The movable mirror is attached to a piston to transfer useful work on the outside environment. Isochoric strokes correspond to energy exchange with phaseonium atoms, while isentropic strokes are driven by mirror displacement. Adjusting the coherence phase  $\phi$  of phaseonium atoms changes the thermalization temperature in the isochoric transformations, enhancing efficiency  $\eta_\phi$  of the engine with respect to one working with classical thermal baths,  $\eta_{cl}$ . (c) Cascade setup: two identical cavities, each with a piston, are sequentially traversed by the same atomic beam, enabling heating or cooling via a shared phaseonium reservoir. The atomic flux is tuned so only one ancilla is in each cavity at a time.

Figure 2 shows the quantum to classical ratio of temperatures  $T_\phi/T_{cl}$ . From this figure, it is clear that for  $2k\pi < \phi < (2k + 1)\pi$  and  $k \in \mathbb{Z}_0$ , given a certain  $\alpha$  within the boundaries of Eq. (1) and Eq. (2), the presence of coherences helps to increase the stable temperature of the pumped cavity. In contrast, for  $(2k - 1)\pi < \phi < 2k\pi$ , the final temperature of the pumped cavity will be lower than in a classical scenario, which means that coherences prevented a full exchange of energy between the ancillas and the cavity. The two temperatures are the same for  $\phi = k\pi$ , when coherences are completely imaginary.

*Methods*— We can exploit this property of coherences to engineer a quantum engine working between two non-thermal temperatures, one higher and one lower than classical, to enhance efficiency.

The same phaseonium baths used to fuel one cavity can interact with more cavities, to scale up the quantum engine. We can arrange cavities one after the another, in a cascade fashion, to let the phaseonium beams interact with them orderly. During the thermalization process, the cavities evolve as one multipartite system, with a unidirectional flow of information mediated by phaseonium atoms. Only when one cavity fully thermalizes, it decouples from the system and does not partake in the evolution any more.

The simplest cycle to perform with a quantum engine is the Otto cycle, represented in Fig. 1(b), where work and heat are

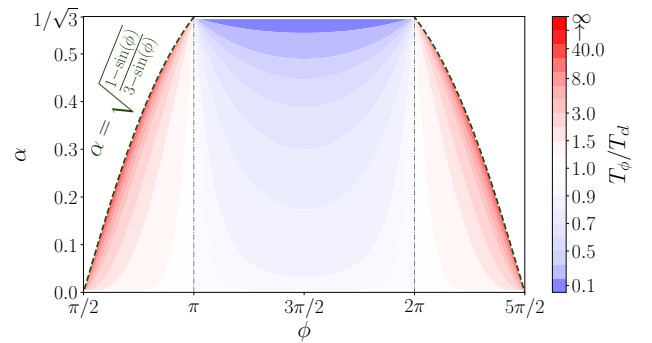


FIG. 2. Ratio between the temperature carried by phaseonium atoms  $T_\phi$  and that of diagonal  $\Lambda$  atoms  $T_{cl}$ . The classical temperature  $T$  is defined only for  $\alpha < \sqrt{1/3}$ , while phaseonium temperature  $T_\phi$  is defined for  $\alpha < \sqrt{(1 - \sin \phi)/(3 - \sin \phi)}$ , limited by the dashed black line represented in the plot. For  $\phi = k\pi$  and  $k \in \mathbb{Z}_0$ , along the dash-dotted grey lines, the two temperatures are the same.

decoupled in different strokes, respectively the two isochoric and the two adiabatic ones. The two adiabatic strokes are guided by phaseonium atoms that carry the apparent phase-dependent temperature, as given in Eq. (1).

For the adiabatic strokes, we use the simplest definition of the pressure operator  $\pi$  [17, 21], to the order  $O((\hat{a}^\dagger \hat{a})^2)$ . As explained in Ref. [19], for a field with frequency  $\omega(t)$  in a

cavity of volume  $V(t)$ , we can define the radiation pressure operator as

$$\pi(t) \equiv \frac{\omega(t)}{2V(t)} \left( \hat{a}^\dagger \hat{a} + \hat{a} \hat{a}^\dagger - \hat{a} \hat{a} e^{-i2\omega t} - \hat{a}^\dagger \hat{a}^\dagger e^{i2\omega t} \right), \quad (3)$$

so that at every time  $t$  we can measure the pressure  $p(t)$  as the expectation value  $\langle \pi(t) \rangle = \text{Tr}[\pi(t)\rho(t)] = \frac{\omega(t)}{V(t)} (\langle \hat{n} \rangle + 1/2)$ , where we can neglect the rotating terms. Considering our system composed of two cavities, for adiabatic strokes we use the global pressure operator  $\pi(t) = \pi_{S_1}(t) \otimes \pi_{S_2}(t)$  associated with the moving cavity mirrors. For an isobaric transformation, the constraint  $\Delta p_n = 0$  dictates the corresponding expansion or compression of the volume  $V(t)$ . In turn, the variable size of the cavity will make the system's Hamiltonian vary in time due to the frequency-length relation  $\omega(t) \propto 1/L(t)$ .

For the isochoric strokes, we employ the full master equation to describe the evolution of the cascade system in contact with the atomic beam.

To characterize the quantum engine, we need to track several metrics. In the simple setup where the engine pushes a piston, we can define the mechanical work  $W^m$  of the engine as the product of the pushing force—i.e. electromagnetic pressure  $p = \text{Tr}\{\rho\pi\}$ —and the displacement of the mirror,

$$W^m = \int_{L_1}^{L_2} p(L) S dL, \quad (4)$$

where  $S$  is the surface area of the cavity and  $L$  is its length, moving from  $L_1$  to  $L_2$ . We can write this in an approximated form explicitly dependent on  $\omega$ . By substituting  $p(L) = \omega$ , neglecting both the rotating terms in Eq. (3) and the zero-point energy, and applying the frequency-length relation  $\frac{dL}{L} = -\frac{d\omega}{\omega}$ , the integration simplifies:

$$W^m = \int_{L_1}^{L_2} \langle \pi \rangle S dL \approx \int_{L_1}^{L_2} \frac{\omega}{L S} \langle \hat{n} \rangle S dL = - \int_{\omega_1}^{\omega_2} \langle \hat{n} \rangle d\omega. \quad (5)$$

This classical expression of work can be compared with the pure quantum equation given by Alicki [22], which stems directly from the first principle of thermodynamics:

$$\frac{d}{dt} \langle H(t) \rangle = \underbrace{\text{Tr} \left[ \rho(t) \frac{dH(t)}{dt} \right]}_{\dot{W}^{\text{AI}}} + \underbrace{\text{Tr} \left[ \frac{d\rho}{dt} H(t) \right]}_{\dot{Q}^{\text{AI}}}. \quad (6)$$

A central figure of merit for thermal machines is their efficiency, defined as the ratio of useful work extracted to the heat absorbed from the hot reservoir. In classical thermodynamics, the upper bound is given by the Carnot efficiency, achievable only in the quasistatic (infinite-time) limit where power output vanishes. To address realistic, finite-time operations, indicators like the Curzon-Ahlborn efficiency [23] were proposed:

$$\eta^{\text{CA}} = 1 - \sqrt{\frac{T_C}{T_H}}. \quad (7)$$

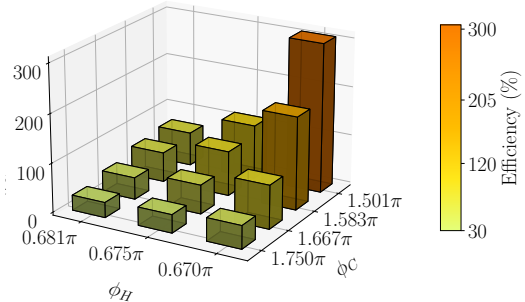


FIG. 3. Ratio between the QE efficiency  $\eta$  and the efficiency of an ideal Curzon-Ahlborn engine  $\eta^{\text{CA}}$  working at the respective classical temperature, for different quantum baths. Hot and cold quantum baths are kept to temperature  $T_\phi^h = 4.8\text{K}$  and  $T_\phi^c = 0.024\text{K}$  respectively. As the hot phaseonium atoms' phase  $\phi_H$  get closer to  $\pi/2$  and the cold atoms' phase  $\phi_C$  goes to  $3/2\pi$ , the efficiency of the quantum engine rises from almost 30%  $\eta^{\text{CA}}$  up to 300%  $\eta^{\text{CA}}$ .

Originally derived for endoreversible engines, it captures the efficiency at maximum power and can be generalized for benchmarking quantum heat engine cycles as well [24].

*Results*— Our engine is made up of one cavity field with a movable mirror fixed to a piston. We employ phaseonium atoms as a quantum thermal bath, characterized by coherence phases  $\phi_H$  for the hot isochore and  $\phi_C$  for the cold isochore. These phases can be precisely tuned to effectively thermalize the cavity field to temperatures exceeding those achievable with classical thermal baths. The operational stability of the engine, given experimental parameters such as the phaseonium-cavity interaction time  $\Delta t$ , interaction strength  $\Omega$ , dimensions of the cavities, and external force  $F$  applied to the piston, is typically achieved within a few operational cycles.

By tuning the coherence phases  $\phi_H$  and  $\phi_C$  according to Fig. 2, we demonstrate significant enhancements in the engine's efficiency compared to a semiclassical thermal bath comprising diagonal  $\Lambda$  atoms (i.e. without coherence between ground states). This advantageous outcome is not merely a theoretical prediction based on comparisons of ideal Carnot or Curzon-Ahlborn efficiencies for engines operating with classical versus quantum baths. Indeed, we robustly confirm it through our realistic implementation utilizing radiation pressure to drive the piston.

We systematically investigated various combinations of phaseonium coherence phases for both the hot and cold thermalization processes, while keeping all other experimental parameters constant. Fig. 3 presents our results, showcasing the ratio between the ideal Curzon-Ahlborn efficiency for an engine operating with two classical baths, and the corresponding efficiency of our quantum engine, working between two quantum phaseonium baths characterized by their coherence phase. The limiting factor here is time, as the cavity requires more time to reach higher or lower temperatures.

If we now plug a second cavity-piston beside the first

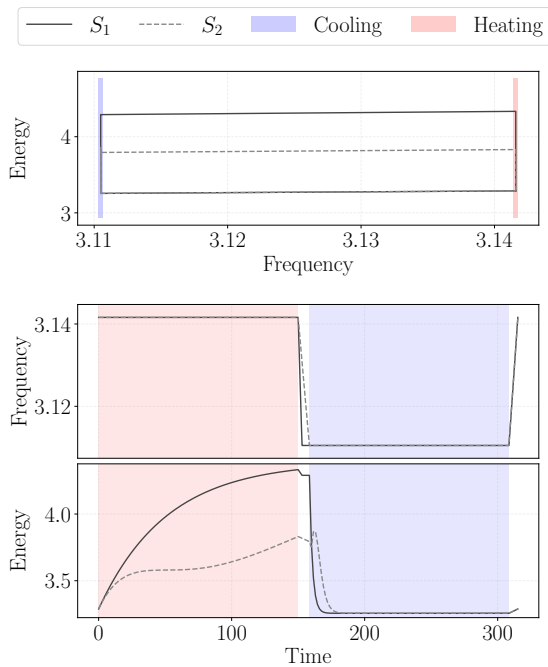


FIG. 4. Regime dynamics of two cavities  $S_1$  and  $S_2$  during one thermodynamical cycle. The hot isochore stroke is not long enough to make the second cavity thermalize, so the two cycles are not equal. In particular, the second cavity performs a smaller cycle, represented with a dashed gray line. Hot phaseonium atoms' coherence phase is set to  $\phi_H = 0.84\pi$ , while for cold atoms  $\phi_C = \pi/40$ . Mutual information shared during expansion is approximately 0.008. The top panel shows the standard Energy-Frequency diagram, typical for an Otto cycle, while the two bottom ones show the dynamics of Frequency and Energy in time. Red and blue bars highlight the heating and cooling processes, respectively.

and thermalize both with the same phaseonium beams as in Fig. 1(c), we double the work output. This again comes at the cost of longer times per cycle, as the second cavity interacts with phaseonium atoms strictly after the first. The second cavity starts to really thermalize only after the first thermalizes and no longer interacts with phaseonium atoms. This is not always desirable, but we can operate the bipartite engine with partial thermalization keeping the same efficiency: while less work is performed, less heat is exchanged with the baths, keeping the efficiency constant. Due to the different temperatures of the cavities coming out of the isochore strokes, they will undergo two different cycles, as seen in Fig. 4.

It is important to keep the transformations of the cavities synchronized, so that during the isochore strokes, the phaseonium beams are resonant with both cavities' frequencies. In this scenario, before the two cavities are both thermalized, they remain correlated through the action of common phaseonium atoms interacting first with the first cavity and then with the second. This action creates a unidirectional flow of information, and thus the mutual information [25] of the bipartite system will be non-zero throughout the cycle, as can be seen in Fig. 5. This means that we can operate with correlated

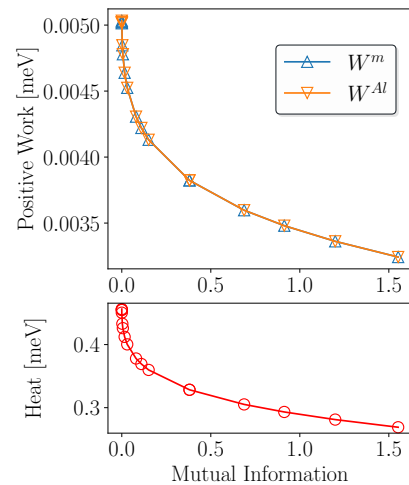


FIG. 5. Comparison of the different definitions of work outputs— $W^m$  and  $W^{Al}$ —and heat absorbed in the hot isochore stroke, for increasing shared mutual information. Mutual information increases by giving less time to the cavities to thermalize: this means less heat absorbed and consequently less work done. The coherence phase of hot and cold phaseonium baths are set to  $0.681\pi$  and  $1.525\pi$ , respectively.

quantum engines without losing efficiency. In Fig. 5, we can also see the agreement of the two work definitions (4) and (6).

*Discussion*— In our simulations, we optimized the parameters to obtain an elongation of the cavity of about 1%. These can obviously be gauged to perform bigger excursions of our piston, but the trade-off is always time. To increase the effects of quantum coherence in the apparent temperature of the cavities, we need to act on the coherence phase of phaseonium atoms and thus slow down the thermalization process. Moreover, slowing the movements of the cavities can reduce the dissipative part of the expansion or compression processes, neglected here. More exact models of pressure forces in a cavity can be found in [26–28]. In the End Matter, we provide an extended discussion on the possible implementations of the proposed engine, referring to experimental values from recent literature to better characterize our model.

In this study, we neglect losses by effectively assuming ideal cavities with infinite  $Q$  factors. However, recent advances in material science have allowed  $Q$  factors as high as  $10^6$  [29]. Photon losses, as well as decoherence, would reduce the efficiency of the quantum engine [14, 16].

Contrary to many quantum engine proposals, our engine does not rely on internal correlations to improve its performance [7, 30–34]. Correlating the two cavities is merely a by-product of scaling the engine to accommodate more pistons. Indeed, we showed that it is still possible to work with correlated and non-thermal systems. Although this may hinder the output of the engine (because less heat is pumped in the engine), the effects on mechanical work may not be as bad as what predicted by the quantum definition, Eq. (6).

*Conclusions*— In this paper, we have proposed a quantum Otto engine composed of two optical cavities operating in parallel, each capable of performing mechanical work on a movable mirror via radiation pressure. The cavities are fuelled by phaseonium atoms, which drive them to an apparent temperature determined by the atomic coherence phase, enabling quantum reservoirs to be engineered to stretch the efficiency limits and improve performances. We have also addressed the problem of *scalability* by adding a second cavity in cascade with the first; this concept can be naturally extended to an array of cavities, all fuelled by the same atomic beam and operating in parallel.

By solving the master equations for the isochoric and adiabatic strokes without approximation, we obtain the exact dynamics of the cycle and track physical metrics such as work and heat throughout the process. This allows a direct comparison between classically defined work and efficiency and their quantum generalizations, providing a benchmark for reconciling quantum and classical thermodynamics.

Phaseonium stands out as the simplest quantum system in which the effects of apparent temperature can be observed, making our scheme both conceptually minimal and experimentally relevant. With current advances in optical cavity technology, the realization of a piston-based optomechanical engine powered by quantum coherence is within reach. Such a device would serve as a testbed for fundamental studies at the quantum–classical interface and could open a path toward scalable quantum engines operating with quantum resources.

*Acknowledgments*— R.L.F. acknowledges support by MUR (Ministero dell’Università e della Ricerca) through the following projects: PNRR Project ICON-Q – Partenariato Esteso NQSTI – PE00000023 – Spoke 2 – CUP: J13C22000680006, PNRR Project QUANTIP – Partenariato Esteso NQSTI – PE00000023 – Spoke 9 – CUP: E63C22002180006. G.A. acknowledges funding from the UK Engineering and Physical Sciences Research Council (EPSRC) under Grant No. EP/X010929/1. F.A. acknowledges the kind hospitality of the University of Nottingham, where part of this work was carried out, and the valuable discussions with Tommaso Tufarelli.

---

\* federico.amato01@unipa.it

† gerardo.adesso@nottingham.ac.uk

‡ rosario.lofranco@unipa.it

- [1] A. Streltsov, G. Adesso, and M. B. Plenio, Quantum Coherence as a Resource, *Rev. Mod. Phys.* **89**, 041003 (2017).
- [2] F. Binder, L. A. Correa, C. Gogolin, J. Anders, and G. Adesso, eds., *Thermodynamics in the Quantum Regime: Fundamental Aspects and New Directions*, Fundamental Theories of Physics, Vol. 195 (Springer International Publishing, Cham, 2018).
- [3] S. Aimet and H. Kwon, Engineering a heat engine purely driven by quantum coherence, *Phys. Rev. A* **107**, 012221 (2023).
- [4] R. Alicki and D. Gelbwaser-Klimovsky, Non-equilibrium quantum heat machines, *New J. Phys.* **17**, 115012 (2015).
- [5] C. L. Latune, I. Sinayskiy, and F. Petruccione, Apparent temperature: demystifying the relation between quantum coherence, correlations, and heat flows, *Quantum Sci. Technol.* **4**, 025005 (2019).
- [6] C. L. Latune, I. Sinayskiy, and F. Petruccione, Roles of quantum coherences in thermal machines, *Eur. Phys. J. Spec. Top.* **230**, 841 (2021).
- [7] C. L. Latune, I. Sinayskiy, and F. Petruccione, Quantum coherence, many-body correlations, and non-thermal effects for autonomous thermal machines, *Sci. Rep.* **9**, 3191 (2019).
- [8] C. Dağ, W. Niedenzu, Ö. Müstecaplıoğlu, and G. Kurizki, Multiatom quantum coherences in micromasers as fuel for thermal and nonthermal machines, *Entropy* **18**, 244 (2016).
- [9] M. O. Scully, From lasers and masers to phaseonium and phasers, *Phys. Rep.* **219**, 191 (1992).
- [10] V. V. Kozlov and J. H. Eberly, Ultrashort pulses in phaseonium: the interplay between sit and eit, *Opt. Commun.* **179**, 85 (2000).
- [11] D. M. Nguyen, C. Soci, and C. H. Ooi, Coherently tunable triangular trefoil phaseonium metamaterial, *Sci. Rep.* **6**, 21083 (2016).
- [12] U. Rathea, M. Fleischhauer, and M. O. Scully, Optical nonlinearities and the kerr-effect in phaseonium, in *Frontiers in Nonlinear Optics, The Sergei Akhmanov Memorial Volume* (CRC Press, 2021) pp. 17–25.
- [13] M. O. Scully, Extracting work from a single heat bath via vanishing quantum coherence ii: Microscopic model, in *AIP Conf. Proc.*, Vol. 643 (American Institute of Physics, 2002) pp. 83–91.
- [14] F. Amato, C. Pellitteri, G. M. Palma, S. Lorenzo, and R. Lo Franco, Heating and cooling processes via phaseonium-driven dynamics of cascade systems, *Phys. Rev. A* **109**, 043705 (2024).
- [15] D. Türkençe and O. E. Müstecaplıoğlu, Quantum fuel with multilevel atomic coherence for ultrahigh specific work in a photonic carnot engine, *Phys. Rev. E* **93**, 012145 (2016).
- [16] H. T. Quan, P. Zhang, and C. P. Sun, Quantum-classical transition of photon-Carnot engine induced by quantum decoherence, *Phys. Rev. E* **73**, 036122 (2006).
- [17] M. Aspelmeyer, T. J. Kippenberg, and F. Marquardt, Cavity optomechanics, *Rev. Mod. Phys.* **86**, 1391 (2014).
- [18] F. Ciccarello, S. Lorenzo, V. Giovannetti, and G. M. Palma, Quantum collision models: Open system dynamics from repeated interactions, *Phys. Rep.* **954**, 1 (2022).
- [19] A. Tejero, D. Manzano, and P. I. Hurtado, An atom-doped photon engine: Extracting mechanical work from a quantum system via radiation pressure, *Phys. Rev. E* **109**, 024141 (2024).
- [20] H.-P. Breuer, F. Petruccione, *et al.*, *The theory of open quantum systems* (Oxford University Press, 2002).
- [21] C. K. Law, Interaction between a moving mirror and radiation pressure: A hamiltonian formulation, *Phys. Rev. A* **51**, 2537 (1995).
- [22] R. Alicki, The quantum open system as a model of the heat engine, *J. Phys. A: Math. Gen.* **12**, L103 (1979).
- [23] F. L. Curzon and B. Ahlborn, Efficiency of a carnot engine at maximum power output, *Am. J. Phys.* **43**, 22 (1975).
- [24] L. M. Cangemi, C. Bhadra, and A. Levy, Quantum engines and refrigerators, *Phys. Rep.* **1087**, 1 (2024).
- [25] W. H. Zurek, Information transfer in quantum measurements: Irreversibility and amplification, in *Quantum Optics, Experimental Gravity, and Measurement Theory*, edited by P. Meystre and M. O. Scully (Springer, 1983) pp. 87–116.
- [26] L. A. S. Machado, P. A. M. Neto, and C. Farina, Quantum radiation pressure on a moving mirror at finite temperature, *Phys. Rev. D* **66**, 105016 (2002).

- [27] E. Cavalcanti and A. P. C. Malbouisson, Quantum forces in cavities, *Phys. Rev. D* **106**, 025005 (2022).
- [28] S. Butera, Corrections to the optomechanical hamiltonian from quadratic fluctuations of a moving mirror, *Phys. Rev. A* **111**, 043524 (2025).
- [29] Q. Qiao, J. Lin, R. Gao, J. Guan, C. Li, G. Zhao, X. Zheng, M. Li, Q. Hou, X. Luo, Y. Qiu, L. Qiao, M. Wang, and Y. Cheng, Integrated high-q cascaded fabry–perot resonators based on lithium niobate sagnac loop reflectors, *Opt. Lett.* **50**, 2370 (2025).
- [30] M. Herrera, J. H. Reina, I. D’Amico, and R. M. Serra, Correlation-boosted quantum engine: A proof-of-principle demonstration, *Phys. Rev. Res.* **5**, 043104 (2023).
- [31] R. S. Watson and K. Kheruntsyan, Quantum many-body thermal machines enabled by atom-atom correlations, *SciPost Phys.* **18**, 190 (2025).
- [32] F. Altintas, A. U. C. Hardal, and O. E. Müstecaplıoğlu, Quantum correlated heat engine with spin squeezing, *Phys. Rev. E* **90**, 032102 (2014).
- [33] Y. Xiao, D. Liu, J. He, Y. Ma, Z. Wu, and J. Wang, Quantum Otto engine with quantum correlations, *Phys. Rev. A* **108**, 042614 (2023).
- [34] A. Hewgill, A. Ferraro, and G. De Chiara, Quantum correlations and thermodynamic performances of two-qubit engines with local and common baths, *Phys. Rev. A* **98**, 042102 (2018).
- [35] S. Kuhr, S. Gleyzes, C. Guerlin, J. Bernu, U. B. Hoff, S. Deléglise, S. Osnaghi, M. Brune, J.-M. Raimond, S. Haroche, E. Jacques, P. Bosland, and B. Visentin, Ultrahigh finesse Fabry-Perot superconducting resonator, *Appl. Phys. Lett.* **90**, 164101 (2007).
- [36] K. J. Vahala, Optical microcavities, *Nature* **424**, 839 (2003).
- [37] F. Famà, S. Zhou, B. Heizenreder, M. Tang, S. Bennetts, S. B. Jäger, S. A. Schäffer, and F. Schreck, Continuous cavity QED with an atomic beam, *Phys. Rev. A* **110**, 063721 (2024).
- [38] A. Suleymanzade, A. Anferov, M. Stone, R. K. Naik, A. Oriani, J. Simon, and D. Schuster, A tunable high-Q millimeter wave cavity for hybrid circuit and cavity QED experiments, *Appl. Phys. Lett.* **116**, 104001 (2020).
- [39] T. Zhang, M. Wu, S. R. Cohen, L. Xin, D. Das, K. K. S. Multani, N. Peard, A.-M. Valente-Feliciano, P. B. Welander, A. H. Safavi-Naeini, E. A. Nanni, and M. Schleier-Smith, Optically accessible high-finesse millimeter-wave resonator for cavity quantum electrodynamics with atom arrays, *Phys. Rev. Appl.* **24**, L041001 (2025).

## END MATTER

### Natural Units for Quantum Simulations

In our numerical simulations, we adopt natural units where  $\hbar = k_B = 1$ . In this framework, all physical quantities are scaled by the cavity’s fundamental frequency  $\omega_0$ . Time is expressed in units of inverse frequency ( $\omega_0^{-1}$ ), and energy and temperature are expressed in units of frequency ( $\omega_0$ ). The cavity length  $L(t)$  is strictly defined by the fundamental resonance condition,  $L(t) = 2\pi c/\omega(t)$ . This allows us to simulate the cycle dynamics in a scale-invariant manner, where results can be mapped to any physical frequency range of interest.

To provide a concrete experimental context for our results, we define a reference frequency scale  $\omega_{\text{ref}}$  based on the physical dimensions of the system. To probe our results on a macroscopic scale, our proposal is the use of macroscopic Fabry–Pérot resonators, which currently achieve cavity lengths  $L$  on the scale of millimeters to centimeters. Accordingly, we select a reference frequency of  $\omega_{\text{ref}} = \omega_0 = 2\pi \times 50$  GHz, corresponding to a fundamental mode wavelength of  $\lambda \approx 6$  mm, to be consistent with the seminal work by S. Kuhr [35]. This choice fixes the physical scales of our dimensionless units: the unit of time maps to  $t_0 = \omega_{\text{ref}}^{-1} \approx 3.18$  ps, while the unit of temperature maps to  $T_0 = \hbar\omega_{\text{ref}}/k_B \approx 2.4$  K. Consequently, a simulation temperature of  $T \approx 1$  corresponds to a physical temperature of 2.4 K, placing our engine in the standard cryogenic regime of microwave cavity QED experiments.

Many different optomechanical platforms can be selected to perform this cycle. Several macroscopic cavity architectures offer distinct geometric and frequency advantages for physically realizing the engine, from cantilever to suspended mirrors to membranes [17]. The canonical standard is established by the superconducting Fabry–Pérot resonators. These can achieve cavity lengths on the scale of millimetres to centimetres, while exhibiting ultra-high quality ( $Q$ ) factors, which indicate strong resilience to photon losses [36, 37]. The canonical superconducting Fabry–Pérot resonator [35] operates at 51.099 GHz, utilizing an open geometry with 50 mm diameter mirrors separated by a 27.57 mm gap. For tighter confinement, seamless 3D crossed-tube niobium cavities operate at 98.2 GHz via intersecting 1.5 mm diameter tubes, forming macroscopic cavities [38]. To balance high cooperativity with necessary transverse optical access, modern near-confocal Fabry–Pérot resonators target the 50 to 100 GHz band, featuring 48 mm diameter mirrors and extended macroscopic gaps up to 47.15 mm [39].